Biosensors and Bioelectronics 154 (2020) 112088

Contents lists available at ScienceDirect

Biosensors and Bioelectronics

journal homepage: http://www.elsevier.com/locate/bios

Iron nanoflorets on 3D-graphene-nickel: A 'Dandelion' nanostructure for selective deoxynivalenol detection

Chong Cheen Ong [a,b], Sangeetha Siva Sangu [a,b], Nabihah Mohammad Illias [a,b], Subash Chandra Bose Gopinath [c,d], Mohamed Shuaib Mohamed Saheed [a,b,*]

[a] Department of Fundamental & Applied Sciences, Universiti Teknologi PETRONAS, 32610, Seri Iskandar, Perak Darul Ridzuan, Malaysia
[b] Centre of Innovative Nanostructures & Nanodevices (COINN), Universiti Teknologi PETRONAS, 32610, Seri Iskandar, Perak Darul Ridzuan, Malaysia
[c] School of Bioprocess Engineering, Universiti Malaysia Perlis, 02600, Arau, Perlis, Malaysia
[d] Institute of Nano Electronic Engineering, Universiti Malaysia Perlis, 01000, Kangar, Perlis, Malaysia

ARTICLE INFO

Keywords:
Aptasensor
Graphene
Iron nanoflorets
Deoxynivalenol
Fusarium

ABSTRACT

Deoxynivalenol (DON), a cosmopolitan mycotoxin found in agricultural commodities causes serious health maladies to human and animals when accidently consumed even at a low quantity. It necessitates selective and sensitive devices to analyse DON as the conventional methods are complex and time-consuming. This study is focused on developing a selective biosensing system using iron nanoflorets graphene nickel (INFGN) as the transducer and a specific aptamer as the biorecognition element. 3D-graphene is incorporated using a low-pressure chemical vapour deposition followed by the decoration of iron nanoflorets using electrochemical deposition. INFGN enables a feasible bio-capturing due to its large surface area. The X-ray photoelectron spectroscopy analysis confirms the presence of the hydroxyl groups on the INFGN surface, which acts as the linker. Clear Fourier-transform infrared peak shifts affirm the changes with surface chemical modification and biomolecular assembly. The limit of detection attained is 2.11 pg mL^{-1} and displays high stability whereby it retains 30.65% of activity after 48 h. The designed INFGN demonstrates remarkable discrimination of DON against similar mycotoxins (zearalenone and ochratoxin A). Overall, the high-performance biosensor shown here is an excellent, simple and cost-effective alternative for detecting DON in food and feed samples.

1. Introduction

Mycotoxins are secondary metabolites with low molecular weight, generated predominantly by fungi from the genera *Fusarium, Aspergillus* and *Penicillium* and commonly invade the crops such as cereal grains, fruits, and even in beer and wine which become a platform for the propagation of fungi and vectors (Eivazzadeh-Keihan et al., 2017; Horky et al., 2018; Santos et al., 2019; Smith et al., 2016). Consequently, mycotoxin causes billions of dollars of loss to the farmers annually and even could cause some crops to be endangered (Srivastava et al., 2018). Mycotoxins are also found in food derived from the animals due to their consumption of the contaminated feeds (Vipotnik et al., 2017).

Due to the omnipresent nature of mycotoxins in food and feed, human and animals are constantly exposed to the risk of ingesting mycotoxin-contaminated food. As a result, human cells and blood affected by mycotoxin lead to severe maladies such as cancer, inflammation, and growth impairments (Eivazzadeh-Keihan et al., 2017). Besides, accidental consumption of feed contaminated with mycotoxins by animals cause growth impairment, weak endocrine system and slowdown of the immune system in them (Gallo et al., 2015). Therefore, the issue of mycotoxin risk needs both agrotechnology and the scientific community's attention (Horky et al., 2018).

Among the major available mycotoxin classes, this study is desired on detecting deoxynivalenol (DON) via biosensor due to its high incidence and severe health effects in humans and animals (Afsah-Hejri et al., 2013). DON is also known as vomitoxin, a group B trichothecene, generally detected in cereal grains at high concentrations. DON is mainly produced by *Fusarium graminearum* in grains and cereals (Ran et al., 2013). In cases of accidental consumption of food and feed contaminated with DON, human and animals suffer from vomiting, gastroenteritis and immunotoxin effects. (Pagkali et al., 2018). Thus, the European Union (EU) has set the maximum allowed limits for DON in food and feed to protect human and animals from the exposure to this mycotoxin (Commission Recommendation 2006/576/EC,

* Corresponding author. Department of Fundamental & Applied Sciences, Universiti Teknologi PETRONAS, 32610 Seri Iskandar, Perak Darul Ridzuan, Malaysia.
E-mail address: shuaib.saheed@utp.edu.my (M.S.M. Saheed).

https://doi.org/10.1016/j.bios.2020.112088
Received 18 November 2019; Received in revised form 7 February 2020; Accepted 8 February 2020
Available online 10 February 2020

2006/576/EC, 2006; Pagkali et al., 2018; Regulation, 2007).

Currently, there are several techniques in detecting DON mycotoxin such as enzyme-linked immunosorbent assay (ELISA) (Lu et al., 2017), lateral-flow immunochromatographic assay (Kong et al., 2019), lateral flow immunoassay (Urusov et al., 2018), and Raman system based sensing (Yuan et al., 2017). Although these techniques demonstrate a good detection limit for DON mycotoxin, the methodologies are complex, time-consuming and costly. The advantages and disadvantages of these conventional methods are summarized in Table S1.

The development of an excellent biosensor requires two important factors, namely selectivity and sensitivity (Lakshmipriya et al., 2013). On top of that, correctly oriented biomolecular immobilization on the sensing surface and minimized non-specific biofouling were also important factors in developing high-performance biosensors. In this study, the biorecognition element was immobilized because the efficiency of non-specific antigen-capturing on the solid surface is lower compared to in-solution-based detection (Cheen et al., 2016). Also to minimize biofouling, the addition of blocking agent on the sensing surface is commonly favoured (Ong et al., 2018). On the other hand, the choice of biorecognition element also plays an important role for selective and sensitive detection. DON-antibody (Huang et al., 2020; Pagkali et al., 2018; Qing et al., 2016; Valera et al., 2019; Wei et al., 2019; Yu et al., 2015) had been widely used as the biorecognition element in detecting DON mycotoxin in the past decades. However, the usage of antibodies as a biorecognition element has its disadvantages in terms of cost, uniformity, affinity control, and shelf-life compared to aptamers (Nimjee et al., 2004).

In the past decades, the development of miniaturized biosensors is possible with the integration of nanostructured materials. Graphene has been a material of interest in various applications such as energy storage (Tang et al., 2019), absorbent (Ong et al., 2019) and sensors (Perumal et al., 2018) since its discovery by Geim and Novoselov. Its unique physical, chemical, optical and electrical characteristics make it an appealing material to be used as a biosensor. There are two approaches to synthesizing graphene, namely the top-down and bottom-up approaches. However, graphene synthesized via top-down approach has major drawbacks such as low specific surface area attribute to the strong π-π interaction between the sheets of graphene (Georgakilas et al., 2012). On the other hand, laser-scribed graphene via bottom-up approach demonstrated a large number of defects and hydrocarbon attachments on the surface of the graphene structure resulting in the deterioration of graphene properties (Vanegas et al., 2018). Recently, alternative techniques in the bottom-up approach such as self-assembly chemical vapour deposition have permitted the development of microporous three-dimensional graphene (Saheed et al., 2017). Graphene produced through this technique possesses fast electron kinetics and large specific surface area; characteristics required for the development of highly sensitive and selective biosensors (Shi et al., 2017). Furthermore, metal oxide nanoparticles have been used for the immobilization of biomolecules due to their biocompatibility (Rahman et al., 2017). Among the metal oxides, iron oxides and (oxy) hydroxides nanoparticles have gained interest due to their unique optical, magnetic, and electrical properties (Ahmed et al., 2019; Rahman et al., 2017). Furthermore, the addition of these metal oxides on the surface of graphene would enhance the active surface area for the attachment of biomolecules and the charge transfer properties.

In this study, DON-aptasensor is developed using a dandelion-like nanostructure, known as iron nanoflorets on the 3D-graphene-nickel substrate as the transducer element and DON-aptamer as the biorecognition element. The 3D-graphene used in this study is synthesized using low-pressure chemical vapour deposition (LPCVD). This strategy benefits the ease of batch fabrication, tunability, and miniaturization. The 3D-graphene will recognize the electrical signal originated by the biomolecular interaction directly using a sensitive dielectric strategy. This is performed by measuring the electrical potential changes that occur on the surface layered with iron nanoflorets. The changes in electrical potential were determined using current-voltage (I–V) measurement. Iron nanoflorets is a promising material for the development of sensitive biosensor due to its high surface area to volume ratio. As for the biorecognition element, a tailor-made aptamer sequence is used for selective detection of DON mycotoxin. The limit of detection (LOD) achieved by the synthesized DON-aptasensor is up to 2.11 pg mL^{-1}.

2. Experimental

2.1. Materials

The nickel foam was acquired from Shanghai Winfay Industry Ltd. Acetone (99.5%), ethanol (70%), iron (II) sulphate, (3-Aminopropyl) triethoxysilane (APTES), glutaraldehyde, phosphate buffer saline (PBS), DON mycotoxin and ethanolamine were purchased from Sigma Aldrich, USA. DON aptamer was synthesized commercially from Apical Scientific Sdn. Bhd. The sequence of aptamer chosen for this study was 5′–NH_2–C6-GCATCACTA-CAGTCATTACGCATCGTAGGGGGGATCGTTAAGGAAGTGCCCG-GAGGCGGTATCGTGTGAAGTGCTGTCCC-3’. All chemicals were stored under the condition recommended by the supplier and used without further purifications.

2.2. Synthesis of iron nanoflorets graphene nickel

The synthesis of graphene followed the previously published report (Saheed et al., 2017). Briefly, nickel foam (2 cm × 2 cm) with 1 mm thickness is cleaned with acetone and isopropanol each for 15 min using sonication to remove organic contaminants. The cleaned nickel foam is placed in the LPCVD furnace at a pressure of 3 Torr (approx. 399.97 Pa) with constant argon and hydrogen flow at 200 and 40 sccm, respectively. The furnace was then heated-up to 1000 °C and maintained for 10 min to stabilize before purging in methane gas at 160 sccm for 20 min for the growth of graphene. Subsequently, iron nanoflorets are decorated on the 3D-graphene surface using electrochemical deposition for 4 min; with pure iron 99.99% as an anode, 3D-graphene as a cathode and iron (II) sulphate as the electrolyte. The obtained iron nanoflorets graphene nickel (INFGN) foam is then washed with deionized water and dried at room temperature.

2.3. Characterization of INFGN

To affirm the synthesis of iron nanoflorets on the 3D-graphene, it is characterized by using field emission scanning electron microscopy (FESEM, Zeiss Supra55 VP) with elemental mapping analysis. X-ray photoelectron spectroscopy (XPS, Model: Thermo Scientific. K-alpha) is used to verify the surface elemental analysis of INFGN with a monochromatic A1 Kα1 source with 1596 eV. The surface modification and biomolecule immobilization are verified by Fourier-transform infrared spectroscopy (FTIR, Model: Pelkin Elmer, Spectrum One) at the range of 200–2500 cm^{-1}.

2.4. Surface chemical functionalization and biomolecular immobilization

The surface chemical functionalization and biomolecular immobilization on the INFGN are performed using the layer-by-layer deposition method. Firstly, the INFGN surface is washed with 70% ethanol to remove impurities from the surface. Once dried, 2.5% APTES is drop coated on the surface of INFGN and incubated for an hour at room temperature. Then, the unreacted APTES is removed by rinsing with 10 folds volume of 10 mM PBS (pH 7.4). To terminate the INFGN surface with aldehyde groups, 3% glutaraldehyde is chemically interacted on the surface and kept for an hour. Next, pre-heated 10 μL of DON aptamer at 92 °C for 2 min is cooled to room temperature and immobilized on the INFGN surface for 30 min. Then, 10 μL of 1 M ethanolamine is applied to the surface for 15 min to block the aldehyde terminated groups that are

not attached by the aptamer. After applying the blocking agent, a drop of diluted DON mycotoxin interacted with the surface for 5 min. DON mycotoxin is diluted in a serial dilution method from 1 ng mL^{-1} to 1 fg mL^{-1} and interaction is carried out independently from the lowest concentration of DON mycotoxin. All washings are performed between each immobilization step with 10 fold volume of PBS.

2.5. Specificity and spiking experiment with real plant sample

For the specificity test, different mycotoxins such as zearalenone (ZEA) and ochratoxin A (OTA) are used to interact on the surface of the aptasensor at a concentration of 1 ng mL^{-1}. For the spiking experiment, paddy (*Oryza sativa*) is crushed with a mortar and pestle to collect its sample and diluted in 1 mL of deionized water. This sample is spiked with 1 mL of 1 ng mL^{-1} of DON and immobilized on the developed aptasensor surface to observe its selectivity towards DON when mixed with plant extract.

2.6. Voltammetry measurements

The current-voltage (I–V) measurement is conducted using picoammeter (Keithley model 6487, 10 fA resolution, voltage source) to determine the electrical conductivity changes after biomolecular interaction and detection. The I–V values for each immobilization step are recorded by applying a voltage sweep (0–2 V). During measurements, the condition is kept as wet and washing steps were carried out between each immobilization/interaction. Every measurement was conducted in a closed chamber with minimum environmental disturbance.

3. Results and discussion

3.1. Field emission scanning electron microscopy

Fig. 1a shows the schematic illustration of iron deposition decorated on the surface of 3D-graphene and its corresponding FESEM image of bare 3D-graphene and INFGN. The growth of dandelion-like nanostructure, iron nanoflorets on the surface of 3D-graphene is observed to be uniform. The elemental mapping of INFGN verifies the uniform elemental distribution of iron and oxygen throughout the surface of 3D-graphene as shown in Fig. 1b. Furthermore, these nanoflorets are uniform in size and distributed on a large surface area, useful to capture a high number of biomolecules. The attachment of iron nanoflorets on the graphene surface is aided by the presence of wrinkles (Ong et al., 2020). The formation of wrinkles is due to the thermal expansion coefficient difference between the nickel and deposited carbon layer (Saheed et al., 2017). The electrons will accumulate at the ridge of the wrinkles and thereby attracts a large number of iron ions to be deposited. This leads to the formation of a dandelion-like nanostructure.

3.2. X-ray photoelectron spectroscopy of INFGN

Fig. 1c and d reveal the narrow scan for Fe2p and O1s regions for INFGN. In the Fe2p region, there are two peaks at 711.88 and 725.18 eV assigned to the $Fe2p_{3/2}$ and $Fe2p_{1/2}$, respectively. The presence of these broad peaks is due to the electrostatic interaction between spin-orbit coupling, photoionized Fe2p core hole, crystal field interaction and Fe3d electrons (Baltrusaitis et al., 2007). The peaks of interest lie in the O1s region, the Fe–O and Fe–OH seen at 530.28 and 531.58 eV, respectively. The presence of hydroxyl groups will provide the necessary binding sites for the attachment of APTES on the surface of INFGN as shown in Fig. 2a.

3.3. Fourier-transform infrared spectroscopy

APTES and glutaraldehyde are used to modify the surface of INFGN as linkers for the attachment of aminated DON-aptamer as shown in Fig. 2a. Initially, the surface is drop-coated with APTES and followed by glutaraldehyde. Subsequently, the DON-aptamer is immobilized on the surface via the glutaraldehyde linker. Fig. 2b shows the FTIR analysis for each surface modification and immobilization steps. APTES attached to

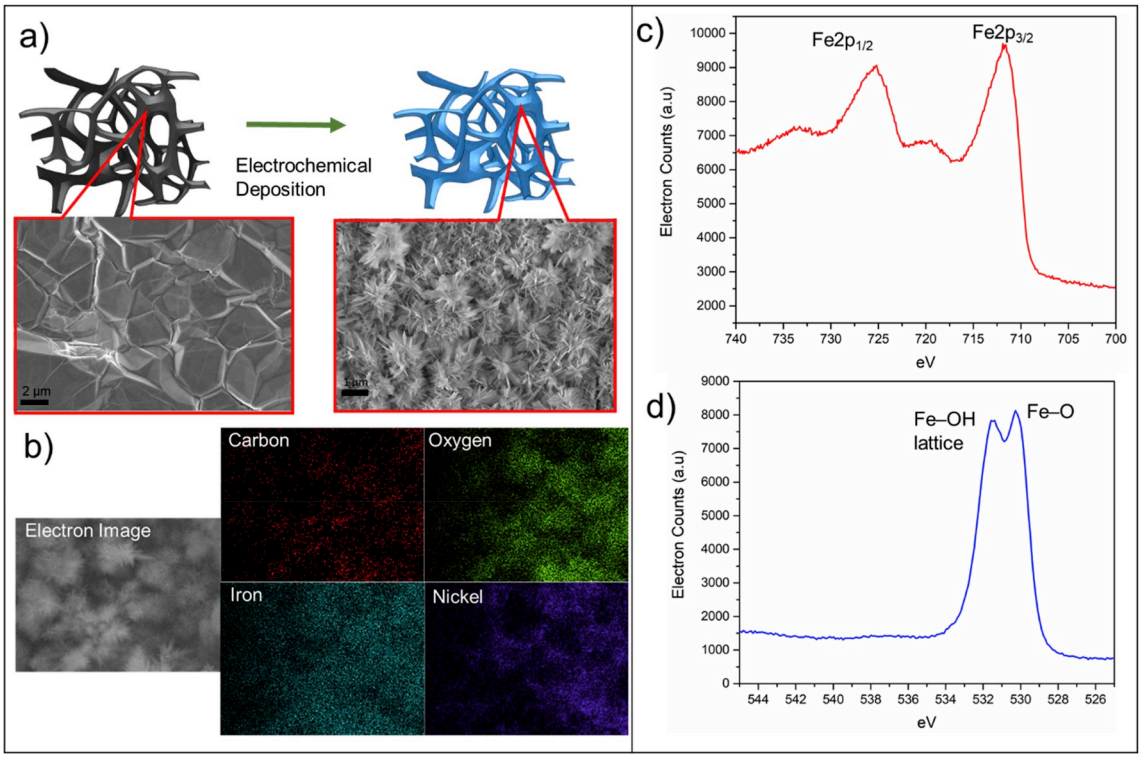

Fig. 1. a) Illustration of electrochemical deposition of iron nanoflorets on 3D-graphene and FESEM image of 3D graphene and INFGN. b) Elemental mapping of INFGN showing the uniform elemental distribution of iron and oxygen throughout the surface of 3D-graphene. Narrow scan of XPS at c) Fe2p region. d) O1s region.

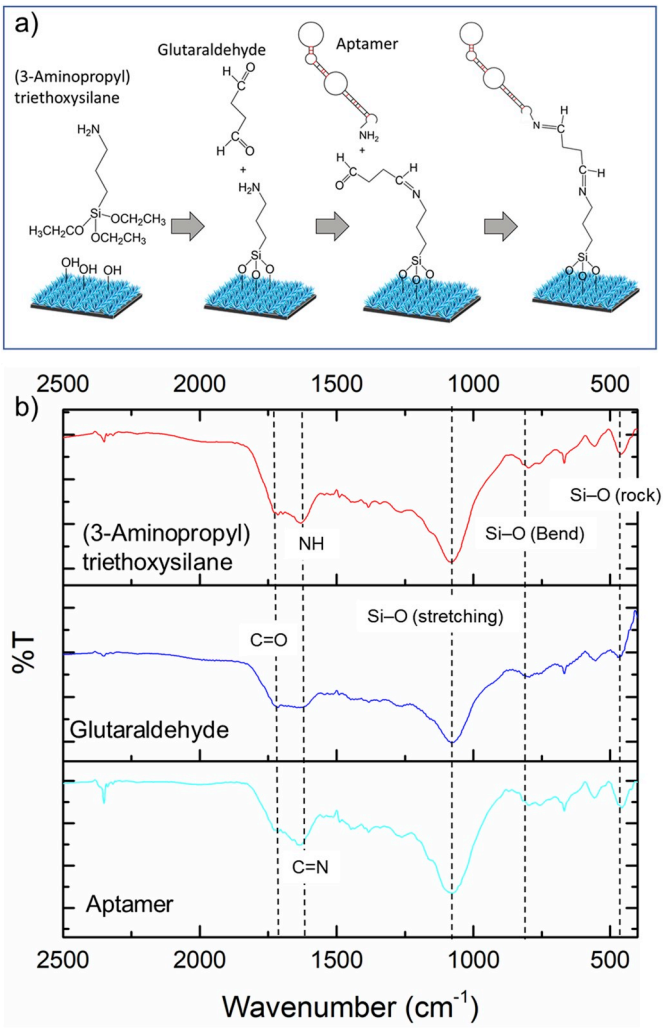

Fig. 2. a) INFGN surface reacted with APTES and glutaraldehyde for the attachment of aptamer. b) FTIR analysis of INFGN with various surface functionalization. Scanned from 200 to 2500 cm^{-1}.

INFGN via hydroxyl groups present on the surface. FTIR spectrum shows the characteristic of Si–O rocking, bending and stretching at 457, 802 and 1081 cm^{-1}, respectively (San Andrés et al., 2000). Besides that, the –NH peaks were also present at 1630 cm^{-1} signifies the NH_2 group of APTES structure (Aneja et al., 2015). Upon the modification by glutaraldehyde, the C═O peak appeared at 1719 cm^{-1}. The broad peak at 1627 cm^{-1} verifies the presence of C═N, which is the linker between APTES and glutaraldehyde. This peak became more prominent as aptamer is attached on the surface via C═N imine bond.

3.4. Electrical potential of INFGN

Fig. 3a shows the reproducibility of the three similar INFGN bare devices based on the reading of current generated through iron nanoflorets at the supplied voltage. The current of the three devices ranges from 0.09 to 0.1 nA. The current generated curve shows a similar trend across all three devices with a relative standard deviation (RSD) of 4.09%.

3.5. Concentration-dependent analysis – LOD determination

Fig. 3b shows the sensitivity of the DON-aptasensor for detecting DON mycotoxin. A range of concentrations from 1 fg mL^{-1} to 1 ng mL^{-1} is used to determine the LOD of DON-aptasensor. The LOD for DON-aptasensor was calculated to be 2.11 pg mL^{-1}, displaying 2 folds higher than the previously reported biosensors (Qing et al., 2016) (Table S3). The current-based LOD determinations for DON as stated by various studies are in the nanoscale range. Although recent studies have reported detecting DON as low as 0.07 pg ml^{-1} using mimotopes, they are comparatively difficult to be produced in addition to the safety concerns and society reluctance to use genetically engineered bacterial viruses (Peltomaa et al., 2017; Yan et al., 2019). In this study, the aptamer is used as the biorecognition element owing to its high specificity, selectivity, and long shelf life compared to the antibodies (Sharma et al., 2016). Initially, the current decreases upon immobilization of aptamer on INFGN as shown in Fig. S1. Fig. 3c shows the biasing of the DON-aptasensor at 2 V, in which the current changes for 10 pg mL^{-1} shows up to 7.7 times difference from the bare DON-aptasensor, signifying the higher sensitivity towards DON mycotoxin. Since DON mycotoxin is a polar compound (Catteuw et al., 2019), electrons can transfer via two pathways; one is through iron nanoflorets and another through the biomolecule (Fig. 3d). Upon addition of DON mycotoxin, it shows improvement in conductivity and a concomitant enhancement has been found by the dose-dependent DON interaction. This proves that the electron opted for the biomolecular pathway with a lower resistance, thus improving the conductivity. A linear increment trend can be observed in the calibration plot (Fig. S2 and Table S2), signifying the higher concentration of biomolecule will increase conductivity up until saturation point. The mechanism of signal generation in the dielectric sensor is the dipole moment, a phenomena when the generated charge displace with strong confinement (Balakrishnan et al., 2014). During the current measurements, the formation of molecular complex structure provoked vibrations, which cause the charge displacement at the dielectric gap.

3.6. Stability and selectivity analysis

Fig. 3e shows the stability results after two days (48 h), where the developed DON-aptasensor is stable and able to maintain 30.65% of its activity. In addition, the selectivity of the DON-aptasensor is determined by using other mycotoxins such as ZEA and OTA. Fig. 3f shows 7 times greater affinity of DON-aptasensor to the DON mycotoxin compared to ZEA and OTA. This shows that DON-aptasensor is very selective towards DON mycotoxin.

3.7. Detection of deoxynivalenol in presence of plant extract-spiking experiment

For the application of plant extract to detect DON, the solution containing 1 mL of plant extract is spiked with 1 ng mL^{-1} of DON mycotoxin as shown in Fig. S3a. DON-aptasensing is prepared similarly with the previous experiment with the plain plant extract dropped on the surface and measured. Evidently from Fig. S3b, there is a negligible current change after the introduction of the plant extract on the DON-aptamer attached surface and showing no affinity towards other compounds in the extract. Meanwhile, the mycotoxin spiked plant extract demonstrates a clear current change at 2 V with 1.5 times of the DON-aptasensor current.

4. Conclusion

In this study, DON-aptasensor is successfully developed with high sensitivity at the LOD of 2.11 pg mL^{-1} and good selectivity (against ZEA and OTA). This DON-aptasensor can maintain its performance of 30.65% after 48 h and able to detect specifically DON mycotoxin in the presence of plant extract. The biosensor developed with the material used in INFGN is achieved through the large surface area of iron nanoflorets coupled with the excellent electrical property of graphene. The addition of aptamer as the biorecognition element instead of antibody and enzyme contributes a consistency in terms of the high-performance.

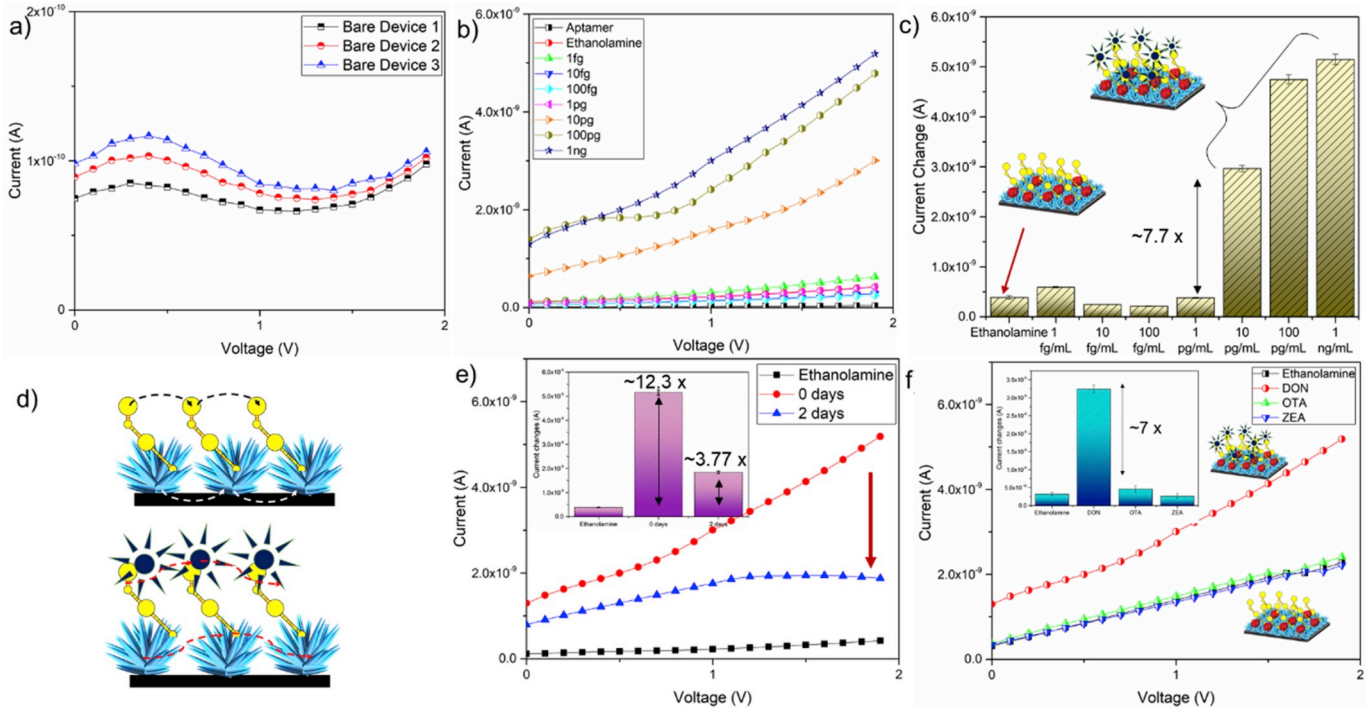

Fig. 3. a) Reproducibility plot. The electrical potential generated by device 1–3 at their bare condition. b) The electrical potential of the DON-aptamer with different concentrations of DON (1 fg mL^{-1} – 1 ng mL^{-1}). c) Current changes at 2 V of different concentrations of DON (1 fg mL^{-1} – 1 ng mL^{-1}). d) Schematic illustration of DON-aptasensor with and without immobilization. e) Stability of DON-aptasensor after 2 days. Inset: Bar diagram of current changes at 2 V. f) I–V measurement shows the selectivity of DON-aptasensor towards the detection of DON and other mycotoxins. Inset: Bar diagram of current changes at 2 V showing the selectivity of DON-aptasensor.

The scheme of using 3D graphene as template for the growth of iron nanoflorets by electrochemical deposition opens new possibilities to use other metal and metal-oxides. This could be useful in improving the stability and reusability of biosensor with addition of targeted surface functionalization. The proposed strategy here provides an excellent platform for future development with graphene-based biosensors as it contains abundance of oxygen species, crucial for attaching linkers and biorecognition elements. It offers a large surface area for the studies of disease biomarkers, especially hazardous mycotoxins plaguing agricultural products.

Declaration of competing interest

The authors declare that they have no known competing financial interests or personal relationships that could have appeared to influence the work reported in this paper.

CRediT authorship contribution statement

Chong Cheen Ong: Methodology, Writing - original draft. **Sangeetha Siva Sangu:** Methodology, Visualization. **Nabihah Mohammad Illias:** Investigation, Validation. **Subash Chandra Bose Gopinath:** Data curation, Writing - review & editing, Project administration. **Mohamed Shuaib Mohamed Saheed:** Conceptualization, Resources, Supervision, Funding acquisition, Project administration, Writing - review & editing.

Acknowledgement

The authors gladfully acknowledge the financial supports by University Research Internal Fund (URIF), Universiti Teknologi PETRONAS with Grant No.: 015LB0-020.

Appendix A. Supplementary data

Supplementary data to this article can be found online at https://doi.org/10.1016/j.bios.2020.112088.

References

Afsah-Hejri, L., Jinap, S., Hajeb, P., Radu, S., Shakibazadeh, S., 2013. Compr. Rev. Food Sci. Food Saf. 12, 629–651. https://doi.org/10.1111/1541-4337.12029.
Ahmed, A., Abagana, A., Cui, D., Zhao, M., 2019. BioMed Res. Int. 14. https://doi.org/10.1155/2019/7127869, 2019.
Aneja, K.S., Bohm, S., Khanna, A.S., Bohm, H.L.M., 2015. Nanoscale 7, 17879–17888. https://doi.org/10.1039/C5NR04702A.
Balakrishnan, S.R., Hashim, U., Letchumanan, G.R., Kashif, M., Ruslinda, A.R., Liu, W. W., Veeradasan, P., Haarindra Prasad, R., Foo, K.L., Poopalan, P., 2014. Sensors Actuators A Phys 220, 101–111. https://doi.org/10.1016/j.sna.2014.09.027.
Baltrusaitis, J., Cwiertny, M., Grassian, V.H., 2007. Phys. Chem. Chem. Phys. 9, 5542–5554. https://doi.org/10.1039/b709167b.
Catteuw, A., Devreese, M., De Baere, S., Antonissen, G., Ivanova, L., Uhlig, S., Martens, A., De Saeger, S., De Boevre, M., Croubels, S., 2019. Arch. Toxicol. https://doi.org/10.1007/s00204-019-02644-x.
Cheen, O.C., Gopinath, S.C.B., Perumal, V., 2016. Microchim. Acta 184, 117–125. https://doi.org/10.1007/s00604-016-2001-6.
Commission Recommendation 2006/576/EC, 2006. Off. J. Eur. Union L 229/7–9, 2005–2007.
Eivazzadeh-Keihan, R., Pashazadeh, P., Hejazi, M., de la Guardia, M., Mokhtarzadeh, A., 2017. TrAC Trends Anal. Chem. 87, 112–128. https://doi.org/10.1016/j.trac.2016.12.003.
Gallo, A., Giuberti, G., Frisvad, J.C., Bertuzzi, T., Nielsen, K.F., 2015. Toxins 7, 3057–3111. https://doi.org/10.3390/toxins7083057.
Georgakilas, V., Otyepka, M., Bourlinos, A.B., Chandra, V., Kim, N., Kemp, K.C., Hobza, P., Zboril, R., Kim, K.S., 2012. Chem. Rev. 112, 6156–6214. https://doi.org/10.1021/cr3000412.
Horky, P., Skalickova, S., Baholet, D., Skladanka, J., 2018. Nanomaterials 8, 727. https://doi.org/10.3390/nano8090727.
Huang, X., Huang, T., Li, X., Huang, Z., 2020. J. Pharmaceut. Biomed. Anal. 177, 112895. https://doi.org/10.1016/j.jpba.2019.112895.
Kong, D., Wu, X., Li, Y., Liu, L., Song, S., Zheng, Q., 2019. Food Chem. 270, 130–137. https://doi.org/10.1016/j.foodchem.2018.07.075.
Lakshmipriya, T., Fujimaki, M., Gopinath, S.C.B., Awazu, K., Horiguchi, Y., Nagasaki, Y., 2013. Analyst 138, 2863–2870. https://doi.org/10.1039/C3AN00298E.

Lu, Y., Wang, S., Yang, J., Qi, M.G., Zhang, Y., Ma, D.-Y., 2017. Food Agric. Immunol. 28, 516–527. https://doi.org/10.1080/09540105.2017.1306491.
Nimjee, S.M., Rusconi, C.P., Sullenger, B.A., 2004. Annu. Rev. Med. 56, 555–583. https://doi.org/10.1146/annurev.med.56.062904.144915.
Ong, C.C., Gopinath, S.C.B., Rebecca, L.W.X., Perumal, V., Lakshmipriya, T., Saheed, M. S.M., 2018. Int. J. Biol. Macromol. 116, 765–773. https://doi.org/10.1016/j.ijbiomac.2018.05.084.
Ong, C.C., Jose, R., Saheed, M.S.M., 2020. Chem. Eng. J. 388, 124306 https://doi.org/10.1016/j.cej.2020.124306.
Ong, C.C., Saheed, M.S.M., Mohamed, N.M., Saheed, M.S.M., 2019. Mater. Today Proc. 16, 1772–1777. https://doi.org/10.1016/j.matpr.2019.06.048.
Pagkali, V., Petrou, P.S., Makarona, E., Peters, J., Haasnoot, W., Jobst, G., Moser, I., Gajos, K., Budkowski, A., Economou, A., Misiakos, K., Raptis, I., Kakabakos, S.E., 2018. J. Hazard Mater. 359, 445–453. https://doi.org/10.1016/j.jhazmat.2018.07.080.
Peltomaa, R., Benito-Peña, E., Barderas, R., Sauer, U., González Andrade, M., Moreno-Bondi, M.C., 2017. Anal. Chem. 89, 6216–6223. https://doi.org/10.1021/acs.analchem.7b01178.
Perumal, V., Saheed, M.S.M., Mohamed, N.M., Saheed, M.S.M., Murthe, S.S., Gopinath, S.C.B., Chiu, J.-M., 2018. Biosens. Bioelectron. 116, 116–122. https://doi.org/10.1016/j.bios.2018.05.042.
Qing, Y., Li, C.R., Yang, X.X., Zhou, X.P., Xue, J., Luo, M., Xu, X., Chen, S., Qiu, J.F., 2016. J. Appl. Electrochem. 46, 1049–1057. https://doi.org/10.1007/s10800-016-0984-7.
Rahman, S.S.U., Qureshi, M.T., Sultana, K., Rehman, W., Khan, M.Y., Asif, M.H., Farooq, M., Sultana, N., 2017. Results Phys 7, 4451–4456. https://doi.org/10.1016/j.rinp.2017.11.001.
Ran, R., Wang, C., Han, Z., Wu, A., Zhang, D., Shi, J., 2013. Food Contr. 34, 138–148. https://doi.org/10.1016/j.foodcont.2013.04.026.
Regulation, (Ec) No 1126/2007 Commission, 2007. No 1126/2007 Comm. Regul 4.
Saheed, M.S.M., Mohamed, N.M., Singh, B.S.M., Saheed, M.S.M., 2017. Diam. Relat. Mater. 79, 93–101. https://doi.org/10.1016/j.diamond.2017.09.004.
San Andrés, E., del Prado, A., Martínez, F.L., Mártil, I., Bravo, D., López, F.J., 2000. J. Appl. Phys. 87, 1187–1192. https://doi.org/10.1063/1.371996.
Santos, A., Vaz, A., Rodrigues, P., Veloso, A., Venâncio, A., Peres, A., 2019. Chemosensors 7, 3. https://doi.org/10.3390/chemosensors7010003.
Sharma, A., Goud, K., Hayat, A., Bhand, S., Marty, J., 2016. Chemosensors 5, 1. https://doi.org/10.3390/chemosensors5010001.
Shi, L., Wang, Y., Ding, S., Chu, Z., Yin, Y., Jiang, D., Luo, J., Jin, W., 2017. Biosens. Bioelectron. 89, 871–879. https://doi.org/10.1016/j.bios.2016.09.104.
Smith, M.C., Madec, S., Coton, E., Hymery, N., 2016. Toxins 8. https://doi.org/10.3390/toxins8040094.
Srivastava, S., Kadooka, C., Uchida, J.Y., 2018. Microbiol. Res. 207, 188–195. https://doi.org/10.1016/j.micres.2017.12.002.
Tang, C., Wang, H.-F., Huang, J.-Q., Qian, W., Wei, F., Qiao, S.-Z., Zhang, Q., 2019. Electrochem. Energy Rev. 2, 332–371. https://doi.org/10.1007/s41918-019-00033-7.
Urusov, A.E., Gubaidullina, M.K., Petrakova, A.V., Zherdev, A.V., Dzantiev, B.B., 2018. Microchim. Acta 185, 29. https://doi.org/10.1007/s00604-017-2576-6.
Valera, E., García-Febrero, R., Elliott, C.T., Sánchez-Baeza, F., Marco, M.P., 2019. Anal. Bioanal. Chem. 411, 1915–1926. https://doi.org/10.1007/s00216-018-1538-0.
Vanegas, D.C., Patiño, L., Mendez, C., Oliveira, D.A. de, Torres, A.M., Gomes, C.L., McLamore, E.S., 2018. Biosensors 8, 42. https://doi.org/10.3390/bios8020042.
Vipotnik, Z., Rodríguez, A., Rodrigues, P., 2017. Int. J. Food Microbiol. 241, 244–251. https://doi.org/10.1016/j.ijfoodmicro.2016.10.031.
Wei, T., Ren, P., Huang, L., Ouyang, Z., Wang, Z., Kong, X., Li, T., Yin, Y., Wu, Y., He, Q., 2019. Food Chem. 300, 125176. https://doi.org/10.1016/j.foodchem.2019.125176.
Yan, J., Shi, Q., You, K., Li, Y., He, Q., 2019. J. Pharmaceut. Biomed. Anal. 168, 94–101. https://doi.org/10.1016/j.jpba.2019.01.051.
Yu, Q., Li, H., Li, C., Zhang, S., Shen, J., Wang, Z., 2015. Food Contr. 54, 347–352. https://doi.org/10.1016/j.foodcont.2015.02.019.
Yuan, J., Sun, C., Guo, X., Yang, T., Wang, H., Fu, S., Li, C., Yang, H., 2017. Food Chem. 221, 797–802. https://doi.org/10.1016/j.foodchem.2016.11.101.